INL EXT-21-64507

# Integration of Dynamical System Scaling to RAVEN and Facility Application

## *Code Implementation and Demonstration*

**September | 2021**

**Ramon Yoshiura**
*Computational Scientist, Integrated Energy & Market Analysis (C170)*

**Aaron Epiney**
*Nuclear/Reactor Engineering, Digital Reactor Technology & Development (C160)*

**Mohammad Abdo**
*Nuclear/Reactor Engineering, Digital Reactor Technology & Development (C160)*

IES
Integrated Energy Systems

*INL is a U.S. Department of Energy National Laboratory operated by Battelle Energy Alliance, LLC*

INL EXT-21-64507

# Integration of Dynamical System Scaling to RAVEN and Facility Application

# Code Implementation and Demonstration

**Ramon Yoshiura**
**Computational Scientist, Integrated Energy & Market Analysis (C170)**
**Aaron Epiney**
**Nuclear/Reactor Engineering, Digital Reactor Technology & Development (160)**
**Mohammad Abdo**
**Nuclear/Reactor Engineering, Digital Reactor Technology & Development (160)**

**September 2021**

**Idaho National Laboratory**
**Integrated Energy Systems**
**Idaho Falls, Idaho 83415**

**http://www.ies.inl.gov**

**Prepared for the**
**U.S. Department of Energy**
**Office of Nuclear Energy**
**Under DOE Idaho Operations Office**
**Contract DE-AC07-05ID14517**

*Page intentionally left blank*

# SUMMARY

As part of the design optimization and model validation effort within the hybrid energy systems program, the research to implement dynamical system scaling (DSS) code to RAVEN is funded under the Integrated Energy System program in collaboration with the Digital Reactor Technology & Development department. The DSS data processing algorithm has been coded within the RAVEN framework along with other metrics and postprocessing models. The implemented code was tested using a gravity-driven draining tank draining case modeled in RELAP5-3D and generated data was successfully postprocessed based on the scaling analyses defined by DSS. Postprocessed data concluded less agreement for the tank exit velocity and indicated that the modeled input deck for RELAP5-3D requires modification to enforce minimal pressure differential effects to the draining process.

*Page intentionally left blank*

# TABLE OF CONTENTS



# FIGURES

## TABLES

*Page intentionally left blank*

# ACRONYMS

| | |
|---|---|
| DSS | dynamical system scaling |
| CMT | core makeup tank |
| TEDS | thermal distribution delivery system |
| NPP | nuclear power plant |
| PWR | pressurized-water reactor |

*Page intentionally left blank*

# Integration of Dynamical System Scaling to RAVEN and Facility Application

## 1. INTRODUCTION

The purpose of this milestone report is to indicate the implementation of dynamical system scaling (DSS) to the RAVEN infrastructure (DSS capabilities integrated in RAVEN are utilized as both postprocessor and metric methodology, enabling the measurement of distance between data sets). The DSS methodology is a time dependent scaling procedure allowing to variate system parameters defined by design objectives, the detection of transient distortions, and unique illustration of generated data. Out of the numerous capabilities provided by DSS, the data synthesis and scaling analyses tools are of particular interest. The utilization of both tools grant users the ability to analyze critical data considering first and second order effects, and the mathematical algorithm to perform such activities are codable. The automation of the proposed DSS capabilities provide users the freedom of repeated usage with minimal knowledge of DSS theory and enables design optimization.

The RAVEN framework is designed to conduct data sampling, reduce order modeling, and postprocessing including various statistical models to flexibly adhere user demands. The code structure developed may sample from user defined codes and it has been demonstrated to interface with external codes. The sampling capabilities provided allows to produce multiple external code inputs for the given distribution and generation method at an instance and fully automated. The combination of RAVEN and DSS can be an effective tool to parametrically investigate key phenomena and lead to design optimization.

One proposed application of the developed DSS code in RAVEN is facility design and test optimization. Applying DSS and other modern scaling techniques to systems and models developed under the Integrated Energy Systems (IES) program constitutes a logic continuation to previous IES work where systems have been analyzed using traditional scaling analysis [7]. As a test case, the facility demonstration will be delivered by conducting scaling analyses for the gravity-driven tank draining process of the core makeup tank (CMT) from Westinghouse AP1000 simulated via RELAP5-3D and downscaled for comparison.

For future applications, the DSS data synthesis or scaling analysis of the secondary side of a typical Westinghouse four loop pressurized-water reactor (PWR) and the thermal energy distribution system (TEDS) is planned.

## 2. BACKGROUND

The development of validation, extrapolation, and scaling of systems is in progress among Purdue University and INL's Digital Reactor Technology & Development group and Integrated Energy & Market Analysis group. By using metric and scaling methodologies such as Representivity [8], Physics-Guided Coverage Mapping [9], and DSS, the main objective is to develop an automatic design optimization model in RAVEN according to user inputs. For energy systems, the platform will quantitatively assess the capability of the energy system models to predict the behavior of nuclear power plants (NPPs), renewable energy, and other multiple generation sources. The collective interaction among various energy sources can be accessible, providing suggestions for efficient hybrid energy design and infrastructure.

One candidate for design optimization is the TEDS facility, part of the Dynamic Energy Transport and Integration Laboratory and under the Integrated Energy System program. One of the missions of the Integrated Energy System organization is to optimize thermodynamic and financial efficiency through systems integration. For the investigation of highly flexible and responsive integrated systems among various energy sources, the Dynamic Energy Transport and Integration Laboratory was established, and tasks such as dynamical electrical balance net generation demand and development of technical methods

to store thermal energy. The TEDS facility is responsible for the thermal systems function to demonstrate the generation, storage, delivery, and use of high-quality energy products to support industrial processes and grid infrastructure [1]. Through the modulation of flow rate and heat input controlled by electrical heaters to emulate steam from NPPs, thermal energy is transferred to heat storage systems or heat customers. This functionality is beneficial for NPPs since the most efficient and economic mode of operation is constant power. If the energy demand requires a ramp-down in power for NPPs, it is unlikely that procedures will be initiated for power adjustments due to possible safety and economic repercussions. The capability to store or sell thermal energy solves the excess energy production while complying with energy demands.

Currently, validation activity for the TEDS model in Dymola (Modelica based) is being conducted utilizing facility data collected from TEDS. The simulation covers transient physics-based models for scaled-up hybrid energy systems, including NPP designs from Westinghouse and NuScale Power. Coupling reactor modules with heat transfer loops to test the feasibility of heat extraction from NPPs will require simulating the system performance in advance. Simulation must be capable of reproducing experimental results. Therefore, a set of representative experiments will need to be defined and used to validate the models against experimental results.

For validation cases like TEDS, the current activity will focus on developing the required framework to use the DSS approach to perform the validation of the simulation model. DSS is an advanced validation methodology that NuScale is already exploring, and it is suggested for validation activities related to the hybridization of the NuScale small modular reactor design. The drain tank simulation noted in the introduction is a verification procedure to test if the DSS methodology has been coded correctly.

## 3. DSS Theory

The origin of the DSS methodology can be found in Reyes 2015 [1] and most of the content shown in this section is introduced in Martin et al. 2019 [2]. The foundation of DSS is derived from general relativity and by parameterizing reference time (the monatomic time measured) using the following calculated term called process time:

$$\tau(t) = \left.\frac{\beta}{\omega}\right|_t$$

where $\beta$ and $\omega$ are the normalized parameter of interest and the agent of change. The normalized parameter of interest is a conserved quantity of the system:

$$\beta(t) = \frac{1}{\Psi_0}\iiint_V \psi(\vec{x},t)\,dV$$

where $\Psi_0$ and $\psi(\vec{x},t)$ are the reference time-independent conserved parameter of interest and localized instantaneous parameter of interest, respectively. The agent of change is the sum of each source differentiating the conserved parameter of interest within the system volume:

$$\omega(t) = \frac{1}{\Psi_0}\frac{d}{dt}\left(\iiint_V \psi(\vec{x},t)\,dV\right) = \iiint_V \left(\phi_v + \phi_f\right)dV + \iint_A (\vec{j}\cdot\vec{n})\,dA - \iint_A \psi(\vec{v}-\vec{v}_s)\cdot\vec{n}\,dA = \sum_{i=1}^{N}\omega_i$$

where $\phi_v$, $\phi_f$, $(\vec{j}\cdot\vec{n})$, $\psi(\vec{v}-\vec{v}_s)$, and $\omega_i$ are the volumetric source or sink, external fields, flux applied to the surface, material transport into or out of the control volume ($v$ is the bulk velocity and $v_s$ is the local instantaneous surface velocity), and i$^{th}$ agent of change ($N$ is the total number of agent of change), respectively. This is also equivalent to the first derivative of the normalized parameter of interest in respect to the reference time:

$$\omega(t) = \left.\frac{d\beta}{dt}\right|_t$$

With the normalized parameter of interest, agent of change, and process time, the new coordinate system is defined to illustrate the distribution of the generated data. Due to general relativity and the geodesic nature of the coordinate system, an invariant postprocessed parameter among the feature and target datasets exists:

$$D(t) = \frac{d\tau - dt}{dt}\Big|_t$$

where $D$ is the temporal displacement rate and is defined as the relative difference between process time and reference time. The sign of the temporal displacement rate describes the relative size of the elapsed process time. If $D > 0$, the system's normalized parameter of interest progression is dilated in comparison with reference time. It is contracted vice versa. When organizing the terms in terms of the variables introduced, the temporal displacement rate is a combination of first- and second-order terms:

$$D(t) = -\frac{\beta}{\omega^2}\frac{d\omega}{dt}\Big|_t$$

Due to the invariant properties, if two datasets' temporal displacement rates are equivalent for each corresponding reference time, it is considered both systems have experienced the same dynamic evolution:

$$D_1(t_1) = D_2(t_2)$$

The progress from one coordinate to another as reference time proceeds is an evolution of the system $(\beta, \omega. \tau)$ phase space. The change in process time dictates the change in the system and is derived as the following:

$$d\tau = \int_{t_I}^{t_F} (D + 1)\, dt$$

This quantity is also called the process action and is used to normalize the magnitude of postprocessed data and adjust the signs depending on process action polarity. Normalized, the following postprocessed data is reformed:

$$\tilde{\beta} = \beta, \tilde{\tau} = \frac{\tau}{\tau_s}, \widetilde{\Omega} = \tau_s \omega, \widetilde{D} = D$$

The normalized parameter of interest and temporal displacement rate are not altered by the process action due to derivations. The scaling is conducted by determining the time scale between the prototype and model time ratio:

$$t_R = \frac{t_M}{t_P}$$

For a time ratio over 1, the time scale of the model is decelerated relative to the prototype. For values below 1, the process is accelerated. To determine the time scale ratio without knowledge of the elapsed prototype and model reference time, the scaling ratio for the parameter of interest and agent of change is the following:

$$\lambda_A = \frac{\beta_M}{\beta_P} = \frac{\widetilde{\Omega}_M}{\widetilde{\Omega}_P}, \lambda_B = \frac{\omega_M}{\omega_P}$$

By applying the reference time prototype and model definition with temporal displacement rate, process time, parameter of interest, and agent of change, the time scaling ratio is alternatively determined as:

$$t_R = \frac{\beta_M \omega_P}{\beta_P \omega_M} = \frac{\lambda_A}{\lambda_B}$$

Depending on the relation between the prototype and model scaling ratios, the type of reference time scaling or process space-time coordinate scaling is found in Table 1.

Table 1: Types of reference time scaling based on parameter scaling ratio [2].

| Basis for Process Space-Time Coordinate Scaling | | | | |
|---|---|---|---|---|
| Metric Invariance | $d\tilde{\tau}_P = d\tilde{\tau}_M$ | And | Covariance Principle | $\frac{1}{\omega_P}\frac{d\beta_P}{dt_P} = \frac{1}{\omega_M}\frac{d\beta_M}{dt_M}$ |
| $\beta - \omega$ Coordinate Transformation | | | | |
| 2-2 Affine $\beta_R = \lambda_A; \omega_R = \lambda_B$ | Dilation $\beta_R = \lambda; \omega_R = \lambda$ | $\beta -$ Strain $\beta_R = \lambda; \omega_R = 1$ | $\omega -$ Strain $\beta_R = 1; \omega_R = \lambda$ | Identity $\beta_R = 1; \omega_R = 1$ |
| Similarity Criteria | | | | |
| $\widetilde{\Omega}_R = \lambda_A$ $\tau_R = t_R = \frac{\lambda_A}{\lambda_B}$ | $\widetilde{\Omega}_R = \lambda$ $\tau_R = t_R = 1$ | $\widetilde{\Omega}_R = \lambda$ $\tau_R = t_R = \lambda$ | $\widetilde{\Omega}_R = 1$ $\tau_R = t_R = \frac{1}{\lambda}$ | $\widetilde{\Omega}_R = 1$ $\tau_R = t_R = 1$ |

The determination of reference scaling type is based on equation scaling conclusions and the objective of the scaling activity. The metric to measure the separation between two associated data points from the prototype and model is along the geodesic lines of constant process time [3]. For every process time, there exist a possible metric characterized as shown in Figure 1 and calculated as the following:

$$\tilde{\eta}(t) = \beta_P(t_P)\sqrt{\varepsilon D_P(t_P)}\left[\frac{1}{\widetilde{\Omega}_P(t_P)} - \frac{1}{\widetilde{\Omega}_M(t_M)}\right]$$

The sum of each temporal separation is the total distortion. To evaluate the overall separation, the standard error based on each local separation is the following:

$$\sigma = \sqrt{\frac{1}{N}\sum_{k=1}^{N}\tilde{\eta}^2(t)}$$

The standard error is also the band of deviation from the constant process time line. Similar to the standard deviation, the measure of dispersion of the mean, the confidence of the data point resides within the band depends on the number of standard errors to observe.

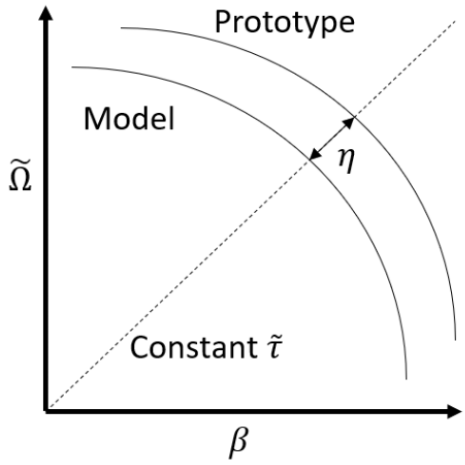


Figure 1. Simple demonstration of process curve separation [4].

## 4. DSS Implementation in RAVEN

To implement DSS into RAVEN, a specific validation gate is prepared to provide the user the flexibility to validate, extrapolate, and optimize. For the DSS validation, we prepared two codes: a postprocessor and metric code. The RAVEN framework illustrated in Figure 2 describes the interaction among systems developed by enabling communication with external codes to perform parametric and stochastic analysis. The postprocessor portion of the DSS code is contained in the models system and receives outputs generated by the external code (which simulates the physics) through the step system. The external code outputs are processed as inputs in the postprocessor and reorganized to enable simple mathematical operations, as introduced in Section 3. The calculation of local separation, total separation, and standard error are reserved for the metrics DSS code residing in the metrics system.

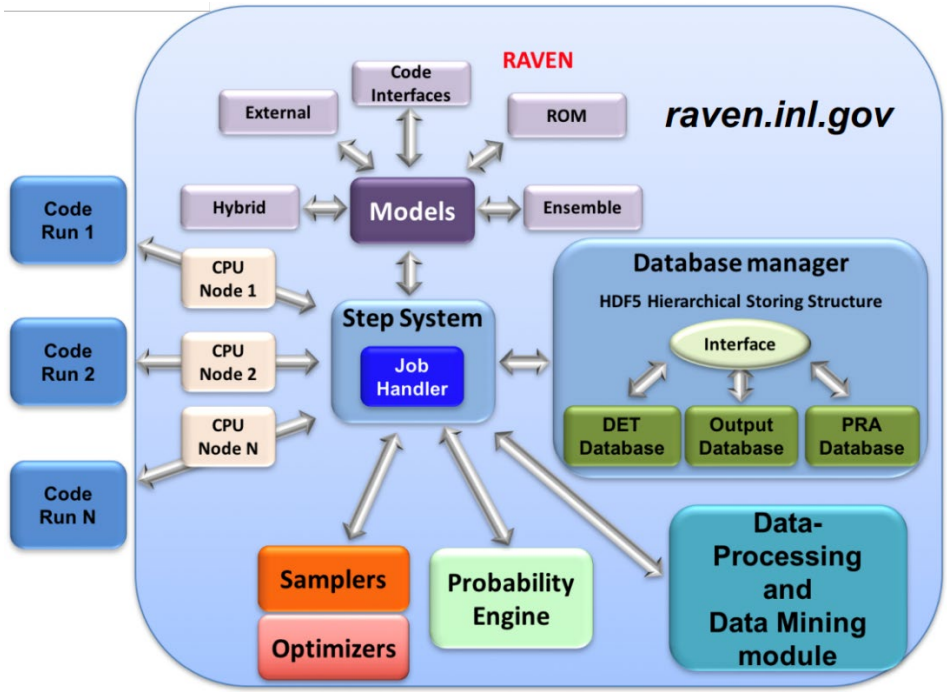


Figure 2. RAVEN framework [5].

## 4.1 RAVEN Workflow of DSS Concept

The DSS code separation is to provide future RAVEN developers the flexibility to access DSS metrics without utilizing the DSS postprocessor code. The concept of the DSS data processing is provided in Figure 3 and describes the basic workflow for a data synthesis case with data sampling for model simulation inputs. The three blocks represent the stages of how the theoretical scaling, RAVEN data handling, and external code data generation interact. The DSS block contains the establishment of figure of merits, exploration of relevant governing equations, and equation scaling to determine the inputs that should be sampled in RAVEN. The interaction between the RAVEN and External block represent communication to generate the sampled data, and postprocess both model and prototype data via DSS postprocessing and metrics code. For all model samples, the model data is compared with a single prototype simulation or experimental generated data and can measure the separation. The postprocessed data are exported as.csv files, and the case of minimal/maximal distortion can be determined.

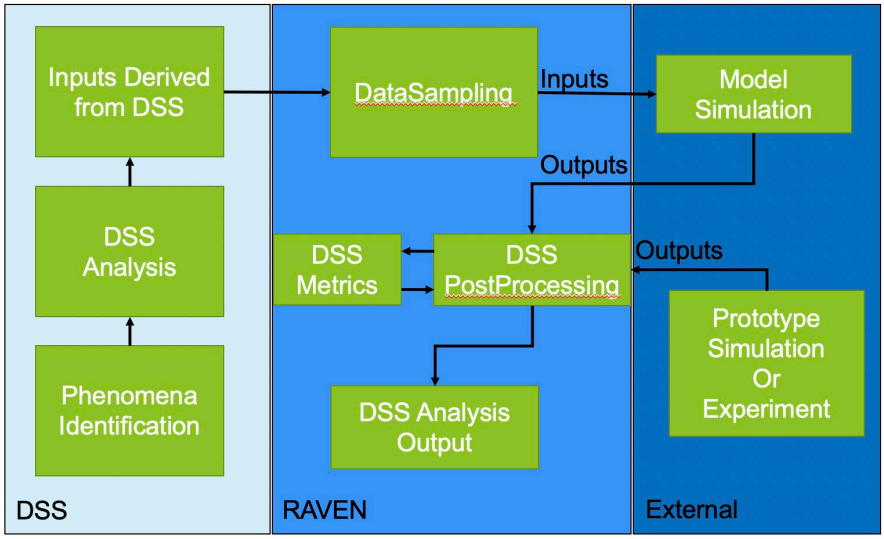


Figure 3. DSS postprocessing concept.

## 4.2 Validation Gate and DSS

The implemented functional code is given in Figure 4 and illustrates the specific interaction between each RAVEN subsystem. Defined by the steps system, the inputs of the external model simulation is supplied by the Sampler system and outputs of the simulation are managed via DataObjects system. If the prototype simulation must be sampled, an additional Sampler step is prepared after the model sampling but before the Postprocessor subsystem to ensure that the data collection is complete. Once the Validation Gate subsystem is initiated, the user is given the choice to select one or more desired validation codes to measure separation between the sampled model and prototype data. The postprocessed data exported by communicating with the OutStreams system to create data printing and plotting. In the future, extrapolation and system optimization codes will be developed to satisfy the project objectives.

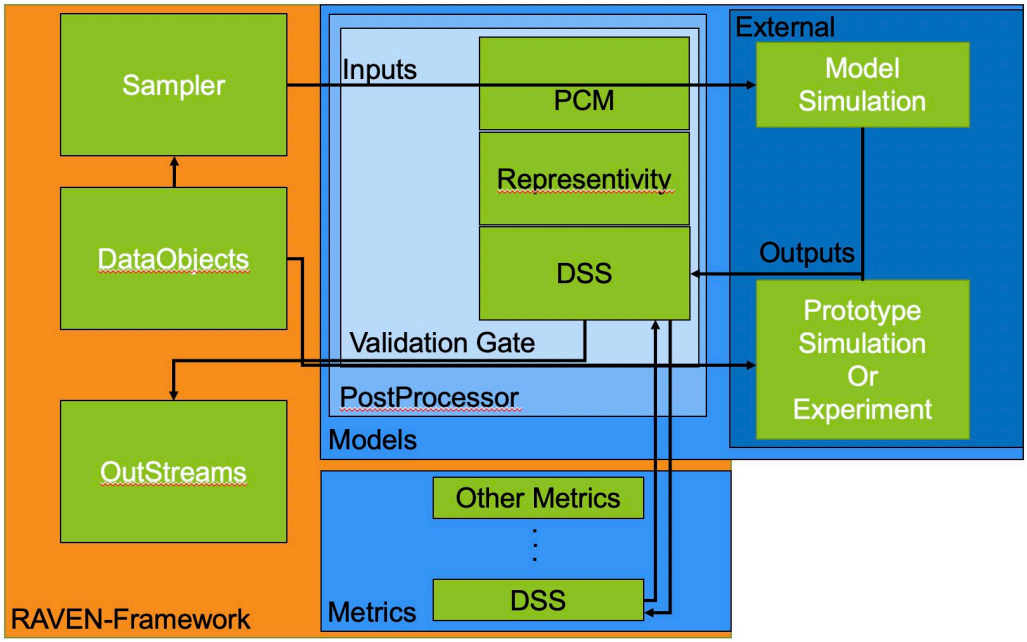


Figure 4. Validation gate and RAVEN information flow chart.

The code unified modeling language diagram for the validation class and DSS metrics is illustrated in Figure 5. For the validation codes, model and prototype data are referred to as features and targets, and may or may not share the same reference time (in RAVEN's case, this is called the pivot parameter) depending on the type of validation code chosen. For the DSS postprocessing code, it further inherits from the validation class. Via the PostProcessorReadyInterface and PostProcessorInterface classes, the validation class is ultimately inherited from the BaseInterface which enables communication with other components in the RAVEN framework without inheriting their class. The essential part of the validation class is the choice of metrics to calculate the corresponding separation between the model and prototype data.

The DSS metrics code resides in the Metrics framework and its sole purpose is to calculate the separation between corresponding reference time or equivalent normalized process time. Since the data from the DSS postprocessor to the DSS metrics is hard coded within the code, the only component the user has control is the choice of time scaling and is a required attribute to define. For time dependent metric codes, the choice of dynamic or piecewise data handling is given to the user to define in the input file. For the case of DSS metrics, the default mode for dynamic handling is true and for piecewise handling is false. Via the MetricInterface, the DSS metric code is also inherited from the BaseInterface and enables efficient data transfer with the validation codes.

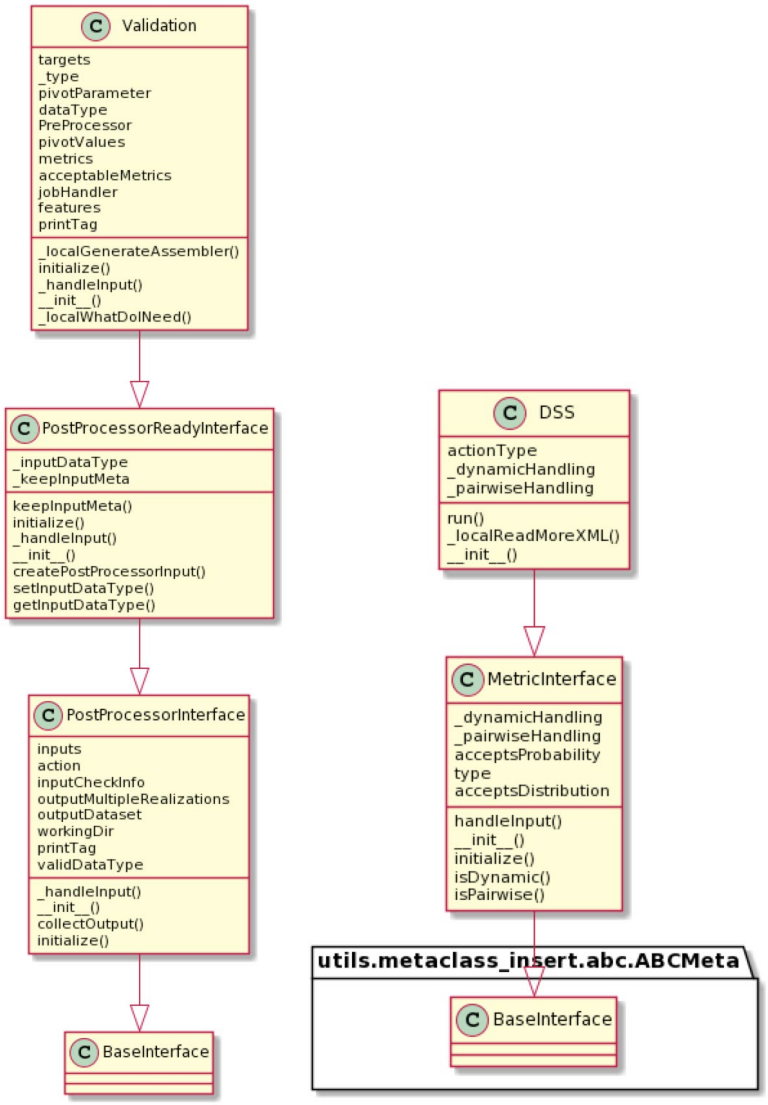


Figure 5 Unified modeling language diagram for the validation and DSS metrics code in RAVEN

# 5. CMT Gravity-Driven Draining RELAP5-3D Test

## 5.1 RELAP5-3D Testing

To test the correct implementation (verification) of the DSS postprocessor and metric code, a core makeup tank gravity-driven draining test introduced by Li et al. [6] is applied. Instead of conducting scaling analyses for both DSS and hierarchical two-tiered scaling for multiple smaller tanks, the DSS code demonstration focuses on a single reduced diameter tank and tests the change in distortion due to variant tank heights. A simple tank hydraulic system was modeled in RELAP5-3D, and Figure 6 shows the nodalisation diagram of the junctions and volumes. The structure is simple; three hydraulic volumes represent the atmosphere, tank, and fluid intercept. All three volumes are set to face vertically upward or 90 degrees inclined from the x and y coordinate plane. By default, the gravitational acceleration is 9.80 $m/s^2$ in the negative direction of the z coordinates. Although, fluid flowing from the bottom to the top of the z coordinates is considered a mass transfer in the positive direction due to orientation, by setting Card 101 for junction entities, the positive flowing direction is altered from top to bottom. To emulate a large volume of air unaffected by the depleting water height of Volume 301, Volume 300 is modeled as a time-

dependent volume with a diameter and height significantly larger than Volume 301 and pressure set to constantly atmospheric. To prevent form loss due to abrupt an area change, the single junction area is adjusted to the top of Volume 301-01. With Volume 300 and Junction 310, the depletion of water level in Volume 301 triggers the suction of air and supplements the loss of water volume. Card 101 in Junction 310 defines the entrance at Volume 300 and exit at Volume 301. This allows RELAP5-3D to recognize the exact location of Junction 310 and resets the positive flowing direction to be -90 degrees from the x-y plane. Volume 301 is the modeled water tank initially filled with water. To track the water level accurately, the volume is expressed as a pipe divided into eight volumes. By recording the void fraction (or fluid volume fraction), the change in each volume is visible, and the sum of all void fractions as a control variable portrays the total water level change, assuming no deformation of the tank (constant tank area). The draining system is simulated by Junction 320 and Volume 302. The area of Junction 320 is half of Volume 301 acting as a circular faucet and medium to atmospheric Volume 302. Card 101 for Junction 320 also defines Word 1 and 2 to reset the positive flowing direction in the negative z orientation. To model an infinite volume of air, identical to Volume 300, the size of Volume 302 is significant in comparison to Volume 301. Table 2 provides the initial and boundary conditions applied in RELAP5-3D.

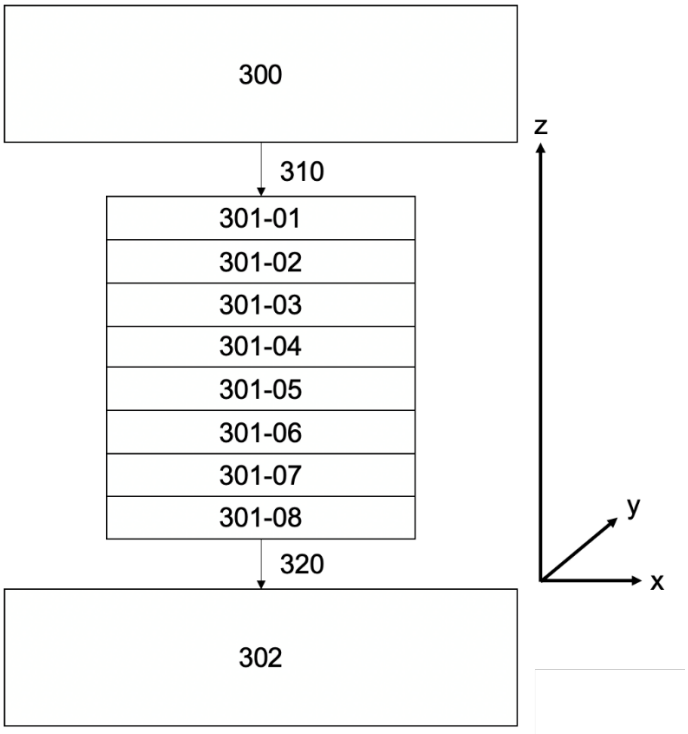


Figure 6. Block diagram of CMT in RELAP5-3D.

The hydraulic system in RELAP5-3D handles only a specie of fluid and gas in a single system. Similar to PWR designs, RELAP5-3D hydraulic systems are isolated from other hydraulics systems. Alternative to mass transport, energy transport via heat transfer is the preferred mode of system-to-system communication. To introduce a two-specie hydraulic system without a phase change due to changes in stored energy, the non-condensable model has been turned on to enable air and liquid water to coexist. As mentioned in the introduction, the draining phenomenon is set to be limited to gravitational effects, and pressure effects have been minimized by placing time-dependent Volumes 300 and 302 with constant atmospheric pressure. For friction effects, while wall friction is considered negligible, form loss due to an abrupt area change remains valid and is calculated internally by RELAP5-3D.

Table 2. RELAP5-3D inputs for CMT.

| Card Number | Type | Void Fraction (air/water) | Initial Condition | Boundary Condition |
|---|---|---|---|---|
| 300 | Time-Dependent Volume | 1.0 | 1 Bar<br>299 K | 1 Bar |
| 310 | Single Junction | N/A | $v_x$: 0.0 m/s<br>$v_y$: 0.0 m/s | N/A |
| 301 | Pipe | 1e-06 | 1 Bar<br>299 K | 1 Bar |
| 320 | Single Junction | N/A | $v_x$: 0.0 m/s<br>$v_y$: 0.0 m/s | N/A |
| 302 | Time-Dependent Volume | 1.0 | 1 Bar<br>299 K | 1 Bar |

## 5.2 Draining Tank Equation

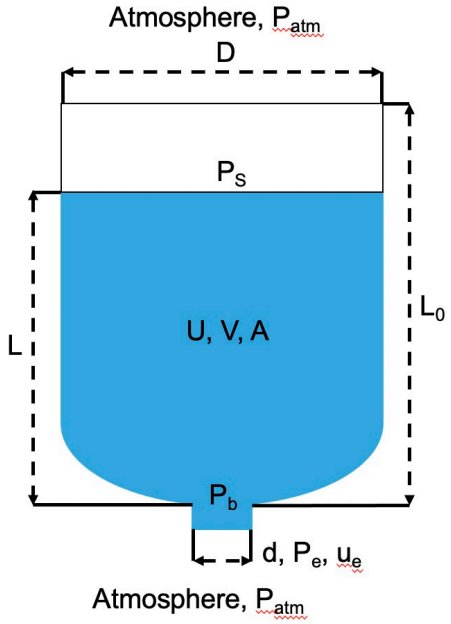


Figure 7. Draining tank.

### 5.2.1 Conservation of Mass

The draining tank geometry is as noted previously in Section 5.1 and in Figure 7. First, the conversation of mass is provided by considering the differential mass and exit velocity outside the faucet:

$$\frac{dm}{dt} = -\dot{m}_e$$

where $m$ and $\dot{m}_e$ are the water mass and exit mass flow rate, respectively. The exit mass flow rate can be replaced with the exit fluid velocity, exit area, water density, tank water velocity, and tank diameter:

$$\frac{dm}{dt} = -\rho u_e A_e = -\rho u A$$

The water mass is expressed as The product of density, length, and area:

$$\frac{dm}{dt} = \frac{d(\rho LA)}{dt}$$

### 5.2.2 Conservation of Momentum

The conversation of momentum considers the pressure, gravitational, friction (excludes form loss since no area change of the tank is considered), advective, and time instantaneous effects:

$$\frac{d(\rho Vu)}{dt} + (\rho uA)u = (P_S - P_b)A + \rho gV - \frac{1}{2}\rho u^2\left(\frac{fl}{D}\right)A$$

where $P_S$, $P_b$, $f$, and $D$ are the water surface pressure, water pressure, friction coefficient, and tank diameter, respectively. Consider Bernoulli's equation with form loss (excludes wall friction) and negligible potential:

$$P_1 + \frac{\rho_1 u_1^2}{2} + \rho_1 g L_1 = P_2 + \frac{\rho_2 u_2^2}{2} + \rho_2 g L_2 + \frac{1}{2}\rho_2 u_2^2 k_2$$

Terms are replaced with Figure 7, assuming the water is incompressible and reorganized:

$$P_b + \frac{\rho u^2}{2} + \rho gL = P_e + \frac{\rho u_e^2}{2} + \frac{1}{2}\rho u_e^2 k_e \rightarrow P_b = P_e + \frac{1}{2}\rho(u_e^2 - u^2) - \rho gL + \frac{1}{2}\rho u_e^2 k_e$$

where $k_e$ is the form loss coefficient due to the abrupt area change. Replace the tank pressure in the conservation of momentum derived from the Bernoulli's equation:

$$\frac{d(\rho Vu)}{dt} + (\rho uA)u = \left(P_S - P_e + \frac{1}{2}\rho(u_e^2 - u^2) - \rho gL + \frac{1}{2}\rho u_e^2 k_e\right)A + \rho gV - \frac{1}{2}\rho u^2\left(\frac{fl}{D}\right)A$$

Reorganize and consider the equivalence in mass flow rate $\left(\dot{m} = \dot{m}_e \rightarrow u_e = u\frac{A}{A_e}\right)$:

$$\frac{d(\rho uV)}{dt} = (P_S - P_e)A - \frac{1}{2}\rho u^2 A\left[(1 + k_e)\left(\frac{A}{A_e}\right)^2 + \left(1 + \frac{fl}{D}\right)\right]$$

Ignore wall friction:

$$\frac{d(\rho uV)}{dt} = (P_S - P_e)A - \frac{1}{2}\rho u^2 A\left[(1 + k_e)\left(\frac{A}{A_e}\right)^2\right]$$

Replace volume with length and area and cancel area and density:

$$\frac{d(uL)}{dt} = \frac{(P_S - P_e)}{\rho} - \frac{1}{2}u^2\left[(1 + k_e)\left(\frac{A}{A_e}\right)^2\right]$$

Apply the chain rule:

$$L\frac{du}{dt} + u\frac{dL}{dt} = \frac{(P_S - P_e)}{\rho} - \frac{1}{2}u^2\left[(1 + k_e)\left(\frac{A}{A_e}\right)^2\right]$$

The alternate version is replacing tank velocity with exit velocity:

$$L\frac{du_e}{dt} + u_e\frac{dL}{dt} = \frac{(P_S - P_e)}{\rho}\frac{A}{A_e} - \frac{1}{2}u_e^2\left[(1 + k_e)\left(\frac{A}{A_e}\right)\right]$$

### 5.2.3 Conservation of Energy

Rearrange Bernoulli's equation with friction loss:

$$P_1 + \frac{\rho_1 u_1^2}{2} + \rho_1 g L_1 = P_2 + \frac{\rho_2 u_2^2}{2} + \rho_2 g L_2 + \frac{1}{2}\rho_2 u_2^2 \left(\frac{fl}{D} + k_2\right)$$

Apply parameters from Figure 7, eliminate pressure effects and wall friction, and cancel density:

$$\frac{u^2}{2} + gL = \frac{u_e^2}{2} + \frac{1}{2}u_e^2 k_e$$

Assume the exit water velocity far exceeds the tank water velocity at any water level ($u_e \gg u$):

$$u_e = \sqrt{\frac{2gL}{1 + k_e}}$$

This result resembles the hierarchical two-tiered scaling energy non-dimensionalization. The reference exit velocity is the time when the tank is full. The form loss remains time-independent, assuming the ratio $A/A_e$ is constant:

$$u_{e0} = \sqrt{\frac{2gL_0}{1 + k_e}}$$

The non-dimensionalizing exit velocity is:

$$u_e^+ = \frac{u_e}{u_{e0}} = \frac{\sqrt{\frac{2gL}{1 + k_e}}}{\sqrt{\frac{2gL_0}{1 + k_e}}} = \sqrt{L^+}$$

## 5.3 DSS Non-Dimensionalization

Starting from the conservation of mass, non-dimensionalize the derived equations:

$$\begin{cases} \dfrac{d(\rho L A)}{dt} = -\rho u_e A_e \rightarrow \dfrac{dL}{dt} = -\dfrac{u_e A_e}{A} \\ \dfrac{du_e}{dt} = -\dfrac{u_e}{L}\dfrac{dL}{dt} + \dfrac{(P_S - P_e)}{\rho L}\dfrac{A}{A_e} - \dfrac{1}{2L}u_e^2\left[(1 + k_e)\left(\dfrac{A}{A_e}\right)\right] \end{cases}$$

Plug in $L = L_0 L_0^+$ and $u_e = u_{e0} u_e^+$:

$$\begin{cases} \dfrac{dL^+}{dt} = -\dfrac{u_{e0} u_e^+ A_e}{L_0 A} \\ \dfrac{du_e^+}{dt} = -\dfrac{u_e^+}{L^+}\dfrac{dL^+}{dt} + \dfrac{(P_S - P_e)}{\rho L_0 L^+ u_{e0}}\dfrac{A}{A_e} - \dfrac{u_{e0} u_e^{+2}}{2L_0 L^+}\left[(1 + k_e)\left(\dfrac{A}{A_e}\right)\right] \end{cases}$$

Eliminate pressure terms:

$$\begin{cases} \dfrac{dL^+}{dt} = -\dfrac{u_{e0} u_e^+ A_e}{L_0 A} \\ \dfrac{du_e^+}{dt} = -\dfrac{u_e^+}{L^+}\dfrac{dL^+}{dt} - \dfrac{u_{e0}}{2L_0 L^+}\, u_e^{+2}\left[(1 + k_e)\left(\dfrac{A}{A_e}\right)\right] \end{cases}$$

Plug in the reference exit velocity:

$$\begin{cases} \dfrac{dL^+}{dt} = -\sqrt{\dfrac{2g}{(1+k_e)L_0}\left(\dfrac{A_e}{A}\right)^2}\, u_e^+ \\ \dfrac{du_e^+}{dt} = -\dfrac{u_e^+}{L^+}\dfrac{dL^+}{dt} - \sqrt{\dfrac{g}{2(1+k_e)L_0}}\dfrac{u_e^{+2}}{L^+}\left[(1+k_e)\left(\dfrac{A}{A_e}\right)\right] \end{cases}$$

Alternatively, plug in $u_e^+ = \sqrt{L^+}$:

$$\begin{cases} \dfrac{dL^+}{dt} = -\sqrt{\dfrac{2g}{(1+k_e)L_0}\left(\dfrac{A_e}{A}\right)^2 L^+} \\ \dfrac{du_e^+}{dt} = -\dfrac{1}{\sqrt{L^+}}\dfrac{dL^+}{dt} - \sqrt{\dfrac{g}{2(1+k_e)L_0}}\left[(1+k_e)\left(\dfrac{A}{A_e}\right)\right] \end{cases}$$

## 5.4 DSS Scaling

For DSS parameters, two parameters of interest and agents of change are defined:

$$\begin{cases} \beta_L = L^+ \\ \beta_{u_e} = u_e^+, \end{cases} \begin{cases} \omega_L = -\sqrt{\dfrac{2g}{(1+k_e)L_0}\left(\dfrac{A_e}{A}\right)^2 L^+} \\ \omega_{u_e} = -\sqrt{\dfrac{g}{2(1+k_e)L_0}\dfrac{A_e}{A}} \end{cases}$$

The temporal displacement rate is the following:

$$\begin{cases} D_L = -\dfrac{\beta_L}{\omega_L^2}\dfrac{d\omega_L}{dt} = -\dfrac{1}{2} \\ D_{u_e} = -\dfrac{\beta_{u_e}}{\omega_{u_e}^2}\dfrac{d\omega_{u_e}}{dt} = 0 \end{cases}$$

The scaling ratios for the parameter of interest, agent of change, and time are:

$$\begin{cases} \lambda_{A,L} = L_R^+ \\ \lambda_{A,u_e} = u_{e,R}^+ = \sqrt{L_R^+}, \end{cases} \begin{cases} \lambda_{B,L} = \sqrt{\dfrac{L_R^+}{L_{0,R}}} \\ \lambda_{B,u_e} = \dfrac{1}{\sqrt{L_{0,R}}} \end{cases}, \begin{cases} t_{R,L} = \sqrt{L_{0,R}} \\ t_{R,u_e} = \sqrt{L_{0,R}}\sqrt{L_R^+} = \sqrt{L_{0,R}}\lambda_{A,L} \end{cases}$$

Depending on the type of time scaling, the values of the scaling ratios vary.

## 5.5 Applied Time Scaling

Two types of time scaling have been selected from Table 1: $\omega$ – strain and identity. Based on the DSS scaling conducted on the mass, momentum, and energy conservation provided in Section 5.4, both water level and exit velocity are initial water level ratio dependent. Each test case for both Sections 5.5.1.2 and 5.5.2.2 are based on the Monte Carlo sampling shown in Table 3.

Table 3. Sampled model parameters for identity and omega strain distortion measurement testing.

| Samples | Model Tank Heights (m) | Reference Exit Velocity (m/s) |
|---|---|---|
| 0 | 22.461 | 19.133 |
| 1 | 19.980 | 18.046 |
| 2 | 31.317 | 22.593 |
| 3 | 22.698 | 19.234 |
| 4 | 14.915 | 15.592 |
| 5 | 1.036 | 4.109 |
| 6 | 26.305 | 20.706 |
| 7 | 24.591 | 20.020 |
| 8 | 15.290 | 15.786 |
| 9 | 25.014 | 20.192 |
| Ideal | 14.000 | 15.106 |

### 5.5.1 Identity

The identity scaling is analogous to the Hierarchical Two-Tiered Scaling when considering the time ratio is maintained to be 1 and the matching of non-dimensional Pi groups between the model and prototype. The following sections will cover the applied time scale, determined geometric dimensions, and yielded results from the simulations and postprocessed data.

#### *5.5.1.1 Scaling*

The constraints for identity from Table 1 are the following:

$$\lambda_A = \lambda_B = t_R = 1$$

To satisfy Section 5.4 conclusions that the model and prototype time ratio is the square root of the tank height ratio, the initial water level ratio is limited to 1 for both water level and exit velocity:

$$t_{R,L} = \sqrt{L_{0,R}} = 1 \rightarrow L_{0,R} = 1$$

Thus, the initial water level of the prototype and model must be the same. Setting the model tank flow area to one fourth (half diameter) of the prototype, the reduced size model tank volume is one fourth of the prototype. Specific dimensions of the prototype and model tank are provided in Table 4.

$$V_M = A_M L_{0,M} = \left(\frac{A_P}{2}\right)\left(L_{0,P}\right) = \frac{V_P}{2}$$

Table 4. Identity scaling prototype and model dimensions.

| | Tank Height (m) | Tank Area ($m^2$) | Nozzle Area ($m^2$) | Form Loss Coefficient |
|---|---|---|---|---|
| Model | 14.00 | 2.00 | 1.00 | 0.204 |
| Prototype | 14.00 | 8.00 | 4.00 | 0.204 |

#### *5.5.1.2 Results*

By sampling 10 different model tank heights (sampled heights are provided in Table 3) via Monte Carlo methods in RAVEN, the distortions were measured for each case. First, the time-dependent normalized raw values are provided in Figures 8 and 9. The water level evolution starts with a filled tank at the normalized water level (raw values divided by the entire tank height) of 1.0 and drains gradually to

a water volume of zero. The discontinuity observed 0.9 normalized water level is due to the pressure differential balancing in the first few hundred milliseconds. The pressure initial conditions for all volumes are 100 kPa. However, when considering the tank will have some hydrostatic pressure initially, RELAP5-3D solver will attempt to rectify pressure and momentarily creates a pressure differential of 91.066 kPa from the top to bottom of the tank (where the pressure is much higher at the top than the bottom). Eventually, after 0.2 seconds, the pressure balances to the correct pressure differential of less than a kPa and is the cause for the discontinuity. For each model case, depending on the tank height, the time to completely drain varies, and as the tank height decreases, the time to drain decreases as well. Keeping in mind the model diameter is half of the prototype (see Table 4) and identity scaling conclusions dictating the draining time to be sync between model and prototype by maintaining the same tank height regardless of tank diameter, the fact that data trends match better approaching the prototype tank height of 14 m agrees with scaling conclusions. Recall, determined by the time ratio derived $t_{R,L} = \sqrt{L_{0,R}}$ and identity scaling condition of $t_{R,L} = 1$ (see Table 1), the ideal derived case is when the model and prototype tank heights are equivalent ($L_{0,M} = L_{0,P}$).

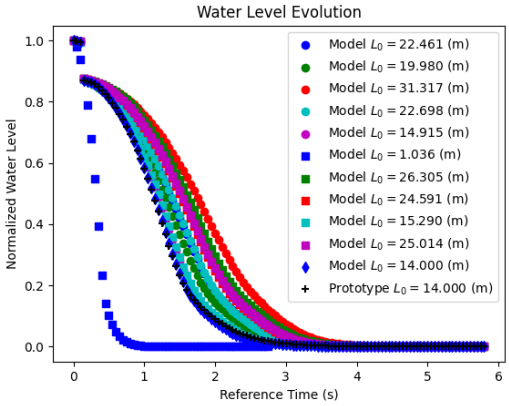


Figure 8. Time-dependent normalized water level for identity time scaling. Each sampled model is provided, and the legend shows the tank height.

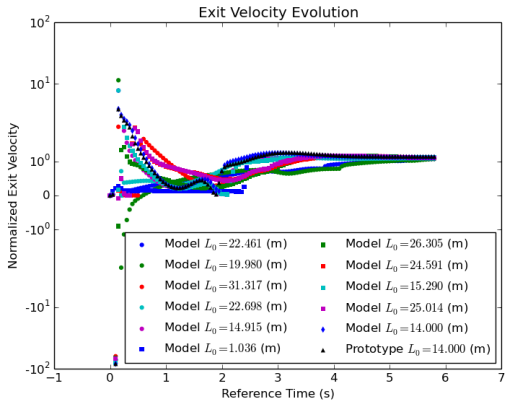


Figure 9. Time-dependent normalized exit velocity for identity time scaling. Each sampled model is provided, and the legend shows the tank height.

For the exit water velocity, as show in Figure 9, the velocity initially reverses due to the pressure discontinuity, returns back to downward flow immediately, and gradually decelerates to realistic values as the pressure differential rectifies. The exit velocity gradually increases until the gravitational acceleration effects are diminished and the flow slows down. Theoretically, the velocity increase is triggered by gravity without wall friction restrictions. Using the derived exit velocity in Section 5.2.3, the exit velocity without starting from the stagnant velocity initial condition. Although the derived exit velocity can only decrease as the water level diminishes, the increase in exit velocity portrays the accelerating water approaching the derived velocity until the potential maximum velocity decreases enough to initiate the water velocity deceleration. The y-axis in Figure 9 is the exit velocity normalized by the reference value (the derived velocity at a fully filled tank) and shows that when excluding the artificial initial transient, the velocity is accelerates at maximum to the reference value. With a similar water level, the ideal scaled case seems closer to the prototype.

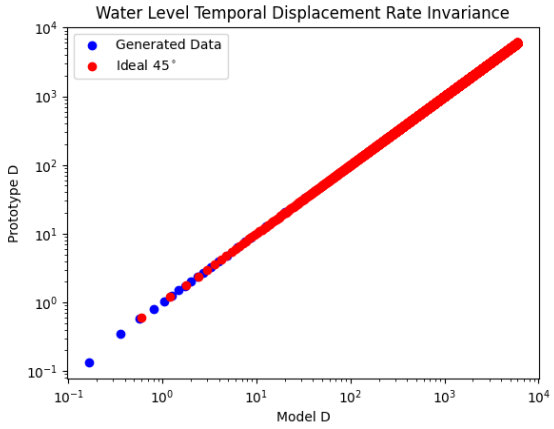


Figure 10. Best matching water level temporal displacement rate at ideal case (identity scaling).

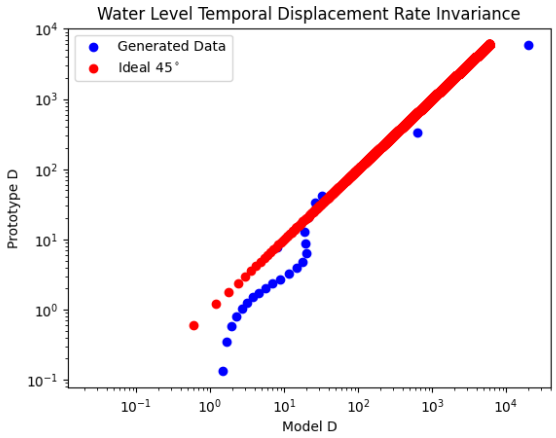


Figure 11. Worst matching water level temporal displacement rate at sample 6 (identity scaling).

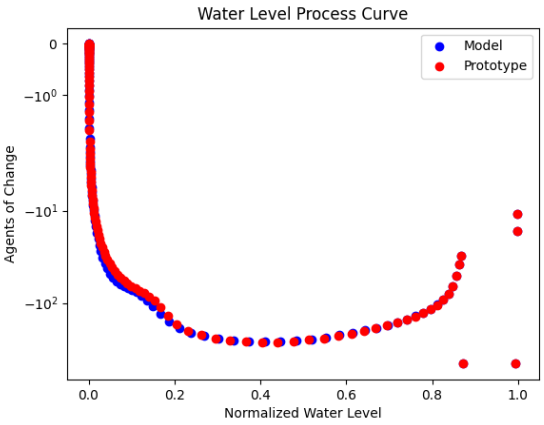


Figure 12. Best matching water level process curve at ideal case (identity scaling).

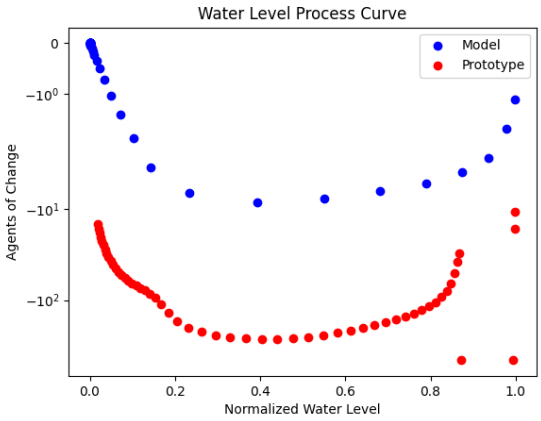


Figure 13. Worst matching water level process curve at sample 5 (identity scaling).

The partial representation of the DSS postprocessed data is shown in Figures 10, 11, 12, and 13 for the best and worst matching cases for the model water level at half diameter and sampled heights. Figure s 10 and 11, illustrate the model and prototype temporal displacement rate and due to the invariant properties, ideally, all model and prototype values must be the same for the corresponding reference times. The unique representation shown in the plots is the comparison with the 45 degree line. If both values are the same, they should follow the 45 degree line at any given point in reference time. Figures 12 and 13, are the process curves as shown in the example in Figure 11. In order for the model and prototype to exist in the same phase space as the same dynamic process, the separation along the constant process time line between both data sets must be minimized. Perfect scaling is defined when these plots completely overlap which can be seen for best matching cases. Based on plot representation, the ideal case had the best agreement and the samples 5 and 6 had the worst. The DSS methodology has successfully expressed the dynamic process in terms of the process space, identified the ideal size derived introduces minimal error, and as the model tank height deviates from the ideal case, expanded the separation between the prototype data. The calculated standard error for water in all cases is provided in Table 5.

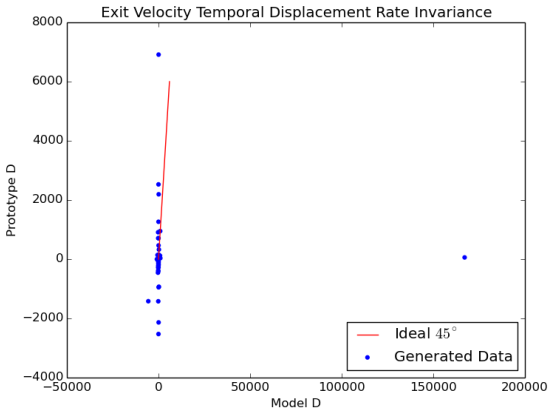


Figure 14. Best matching exit velocity temporal displacement rate at ideal case (identity scaling).

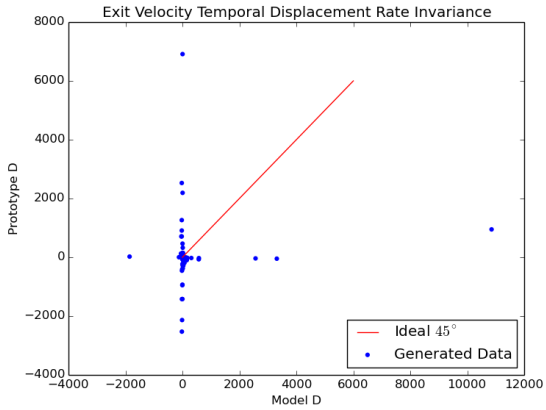


Figure 15. Worst matching exit velocity exit temporal displacement rate at sample 6 (identity scaling).

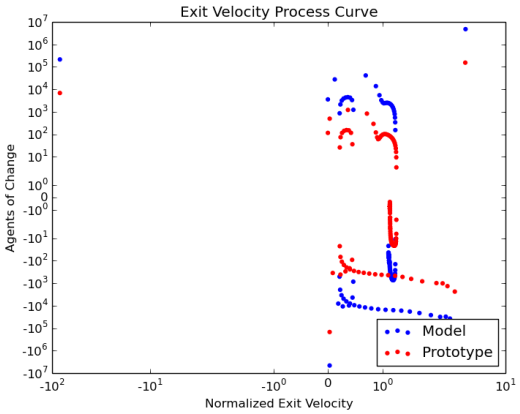


Figure 16. Best matching exit velocity process curve at ideal case (identity scaling).

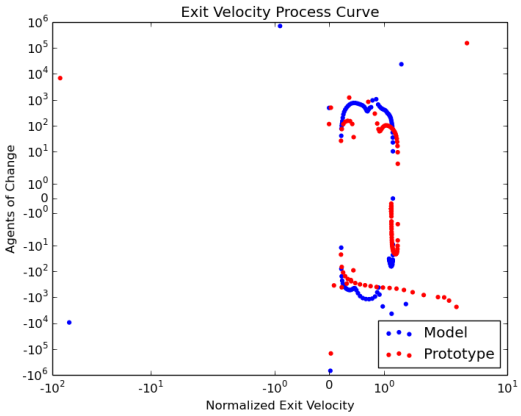


Figure 17. Worst matching exit velocity process curve at sample 6 (identity scaling).

The partial representation of the DSS postprocessed data is shown in Figures 14, 15, 16, and 17 for the best and worst matching cases for the model exit velocity. DSS methodology has successfully expressed the dynamic process in terms of the process space and temporal displacement rates matched relatively well. When comparing Figures 16 and 18, the trend and normalized exit velocity distribution represented for the derived ideal case strongly resembles the prototype case. The issue is that the magnitude of the exit velocity normalized agents of change. The magnitude is controlled by calculating the process action, which is the integral of the temporal displacement rate in respect to reference time. By observing the non-normalized agents of change, the values are close in magnitude and represent similar behaviors (the first derivative of Figure 9). The identity scaling ensured that, by keeping equivalent tank heights, the draining timing is synced. The comparison of draining times reveal that the mismatch of tank height can either over- or underpredict the total draining elapsed time. To correct the ideal simulation overlapping with the prototypic exit velocities, the second-order gradients must be close enough to

guarantee a minimal data separation. The calculated standard error for water of all cases is provided in Table 5.

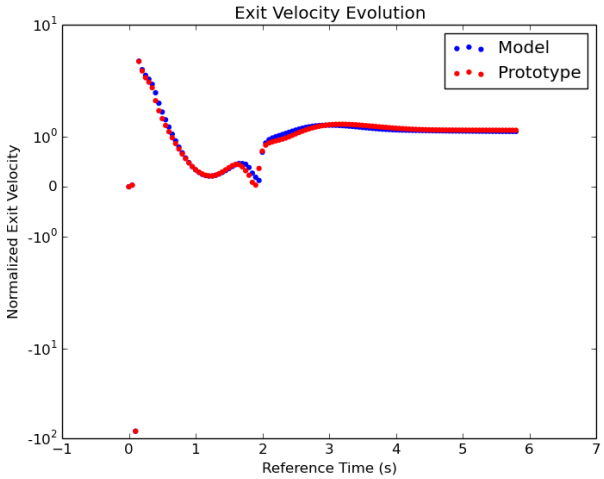


Figure 18. Exit velocity evolution for the derived ideal case (identity scaling).

Overall, the draining tank identity scaling demonstrated a minimal standard error for water level. To determine minimal distorted case for exit velocity, the RELAP5-3D input deck modification is required to eliminate the initial differential pressure transient and exclude sources of error. The best method to improve exit velocity scaling is to consider and model hydrostatic pressure as the initial boundary condition in card 301. Exit velocity standard error will be further minimized after input deck modifications.

Table 5. Identity water level and exit velocity standard errors for each sampled case.

| Samples | Tank Height (m) | Water Level Standard Error | Exit Velocity Standard Error |
|---|---|---|---|
| 0 | 22.461 | 1.949e-1 | 18.383 |
| 1 | 19.980 | 1.663e-1 | 19.048 |
| 2 | 31.317 | 2.669e-1 | 20.729 |
| 3 | 22.698 | 1.997e-1 | 20.390 |
| 4 | 14.915 | 2.322e-2 | 20.794 |
| 5 | 1.036 | 5.723 | 7.067 |
| 6 | 26.305 | 2.229e-1 | 20.489 |
| 7 | 24.591 | 4.843e-1 | 20.501 |
| 8 | 15.290 | 3.613e-2 | 20.530 |
| 9 | 25.014 | 4.854e-1 | 20.593 |
| Ideal | 14.000 | 2.896e-4 | 20.691 |

### 5.5.2 $\omega$ – Strain

The $\omega$-strain scaling is capable of accelerating and decelerating a process by simply setting the agents of change scaling ratio less or greater than 1. Due to scaling conditions, the normalized parameter of interest scaling is maintained to be 1. The following sections will cover the applied time scale, determined geometric dimensions, and yielded results from the simulations and postprocessed data.

#### 5.5.2.1 Scaling

The constraints for identity from Table 1 are the following:

$$\lambda_A = 1, \lambda_B = \lambda, t_R = \frac{1}{\lambda}$$

To satisfy Section 5.4 conclusions and by setting the water level agent of interest scaling ratio to be $\sqrt{2}$ ($\lambda_{B,L} = \sqrt{2}$), the initial water level ratio is limited to one fourth for both water level and exit velocity:

$$t_{R,L} = \sqrt{L_{0,R}} = \frac{1}{\sqrt{2}} \rightarrow L_{0,R} = \frac{1}{2}$$

Thus, the initial water level of the model is half of the prototype. Applying a geometric similarity, where the model tank diameter is half of the prototype, the reduced size model tank area is one fourth and one eighth of the prototype. Specific dimensions of the prototype and model tank are provided in Table 5:

$$D_M = \frac{D_P}{2} \rightarrow A_M = \frac{A_P}{4} \rightarrow V_M = A_M L_M = \left(\frac{A_P}{4}\right)\left(\frac{L_P}{2}\right) = \frac{V_P}{8}$$

Table 6. $\omega$ – Strain scaling prototype and model dimensions.

| | Tank Height (m) | Tank Area ($m^2$) | Nozzle Area ($m^2$) | Form Loss Coefficient |
|---|---|---|---|---|
| Model | 7.00 | 2.00 | 1.00 | 0.204 |
| Prototype | 14.0 | 8.00 | 4.00 | 0.204 |

#### 5.5.2.2 Results

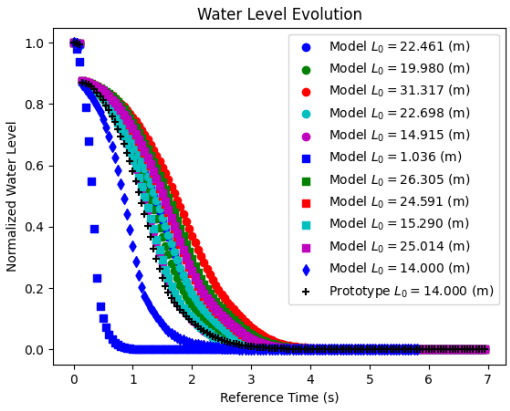


Figure 19. Time-dependent normalized water level for *ω-strain* time scaling. Each sampled model is provided, and the legend shows the tank height.

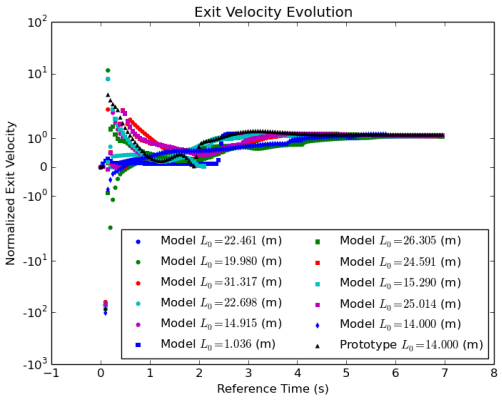


Figure 20. Time-dependent normalized exit velocity for ω-*strain* time scaling. Each sampled model is provided, and the legend shows the tank height.

The discontinuity observed 0.9 normalized water level is due to the same pressure differential adjustments in the identity scaling, and the pressure balance initiates the realistic continuous behavior of draining water. The distortions measured for each case are the same identity scaling samples with an applied time scaling ratio to adjust the model reference time. As explained in Section 5.5.1.2, the water

level evolution starts with a filled tank at a normalized water level, drains gradually to zero water volume, each model case draining time varies depending on the tank height. Dictated by the scaling conducted in Section 5.5.1.1 to accelerate the draining process $\sqrt{2}$ times faster by reducing the tank height by half, it is expected the model draining time until zero water volume to be less than the he prototype. Although it is difficult to judge from Figures 19 and 20 which data set matches best with the prototype, Table 7 presents the standard error for all cases. Sample 8 standard deviation is the minimal distorted case, and its height is near the prototypic height suggests pressure effects to exit velocity may influence the draining level more significantly than anticipated.

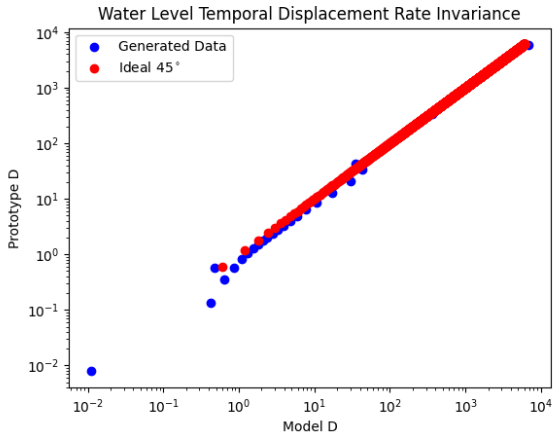


Figure 21. Best matching water level temporal displacement rate at sample 4 ($\omega$-strain scaling).

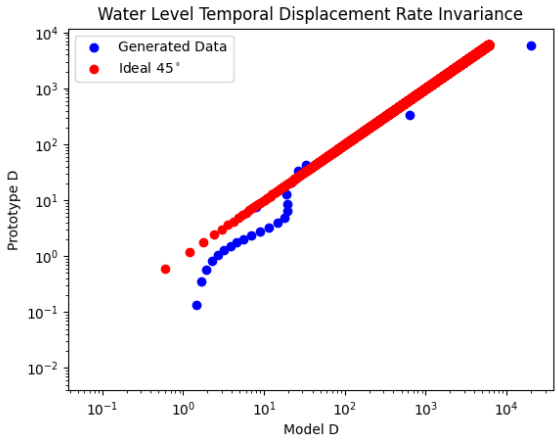


Figure 22. Worst matching water level temporal displacement rate at sample 6 ($\omega$-strain scaling).

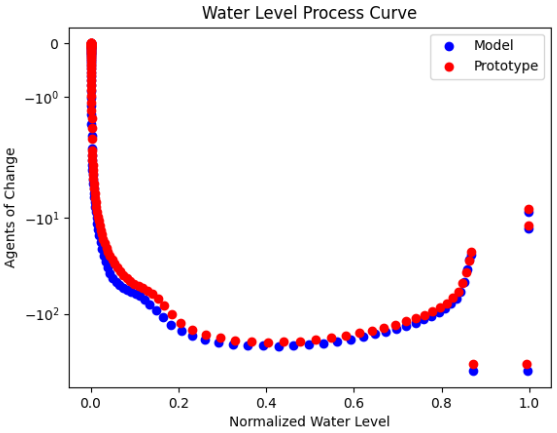


Figure 23. Best matching water level process curve at sample 4 ($\omega$-strain scaling).

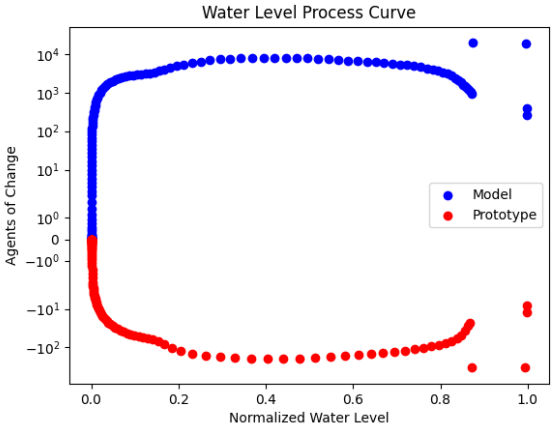


Figure 24. Worst matching water level process curve at sample 6 ($\omega$-strain scaling).

For the exit water velocity, as shown in Figure 20 and in Section 5.5.1.2, reversed flow is observed due to the initial pressure discontinuity, and is immediately rectified to normal distributions. Same as the identity scaling, gradual increase then a gradual decrease in exit velocity is shown due to the close relationship between remaining water level and gravitational acceleration. Excluding the initial pressure discontinuity affected velocity, the exit velocity behaves well within the reference value derived (normalized exit velocities below the value of 1). Although it is contrary to the scaling conclusion that a tank height of 7

meters would ideally represent the prototype accelerating the draining process by 30%, cases that nearly matched the prototype tank height indicated better agreement than derived ideal case.

The partial representation of the DSS postprocessed data is shown in Figures 21, 22, 23, and 24 for the best and worst matching cases for the model water level at half diameter and sampled heights. As explained in the identity scaling results, overlapping data of the temporal displacement rate and process curve is indication of good agreement, and vice versa. Following this basic rule, sample 4 has the best and sample 6 has the worst agreement. the DSS methodology has successfully expressed the dynamic process in terms of the process space, identified that the ideal size derived did not introduce minimal error, and suggested that the cases with similar prototypic tank heights (sample 4) minimize the standard error. The calculated standard error for water in all cases is provided in Table 7.

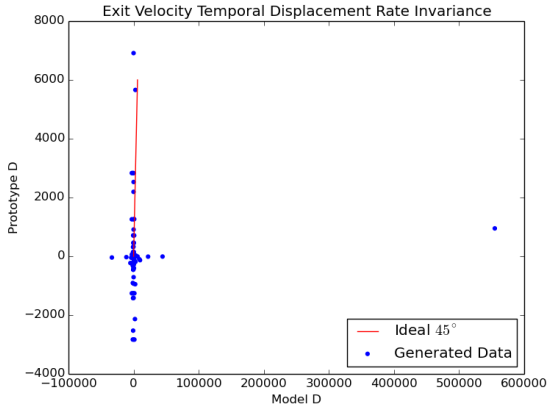


Figure 25. Best matching exit velocity temporal displacement rate at sample 4 ($\omega$-strain scaling).

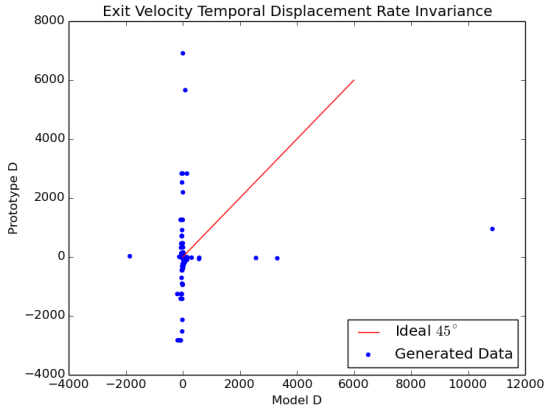


Figure 26. Worst matching exit velocity exit temporal displacement rate at sample 6 ($\omega$-strain scaling).

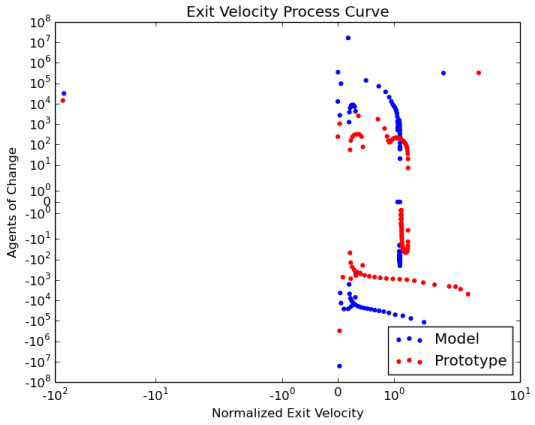


Figure 27. Best matching exit velocity process curve at sample 4 ($\omega$-strain scaling).

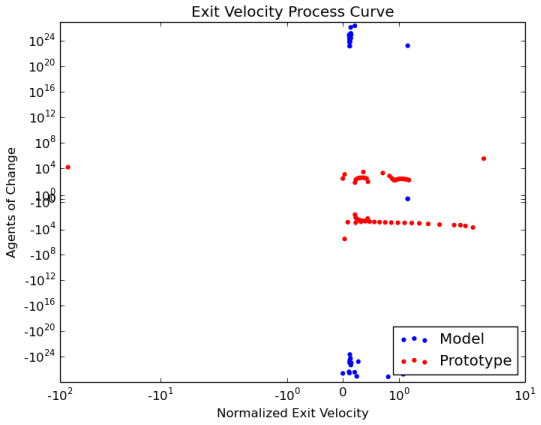


Figure 28. Worst matching exit velocity process curve at sample 5 ($\omega$-strain scaling).

The partial representation of the DSS postprocessed data is shown in Figures 25, 26, 27, and 28 for the best and worst matching cases for the model exit velocity. DSS methodology has successfully

expressed the dynamic process in terms of the process space and temporal displacement rates matched relatively well. When comparing Figures 29 and 30, the difference on how well the two models resembled the prototype is visible. Although the scaling predicted Figure 29 to be the case with minimum separation, Figure 30 indicated higher levels of resembles to the prototype trend, and it is possible pressure effects due to height difference may potentially drive the draining process when tank height differences exist between the model and prototype. The calculated standard error for water in all cases is provided in Table 7.

The partial representation of the DSS postprocessed data is shown in Figures 14, 15, 16, and 17 for the best and worst matching cases for the model exit velocity. DSS methodology has successfully expressed the dynamic process in terms of the process space and temporal displacement rates matched relatively well. When comparing Figures 16 and 18, the trend and normalized exit velocity distribution represented for the derived ideal case strongly resembles the prototype case. The issue is that the magnitude of the exit velocity normalized agents of change. The magnitude is controlled by calculating the process action, which is the integral of the temporal displacement rate in respect to reference time. By observing the non-normalized agents of change, the values are close in magnitude and represent similar behaviors (the first derivative of Figure 9). The identity scaling ensured that, by keeping equivalent tank heights, the draining timing is synced. The comparison of draining times reveal that the mismatch of tank height can either over- or underpredict the total draining elapsed time. To correct the ideal simulation overlapping with the prototypic exit velocities, the second-order gradients must be close enough to guarantee a minimal data separation. The calculated standard error for water of all cases is provided in Table 5.

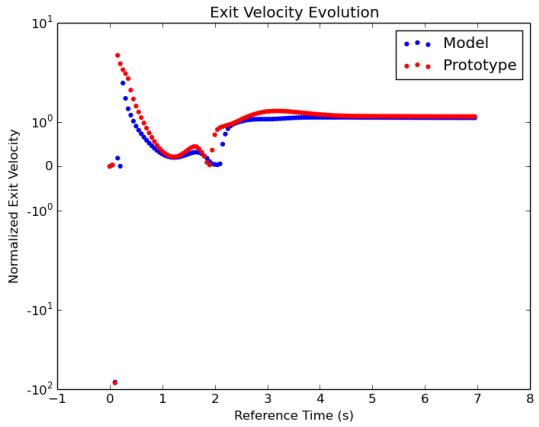


Figure 29. Exit velocity evolution of sample 4 ($\omega$-strain scaling).

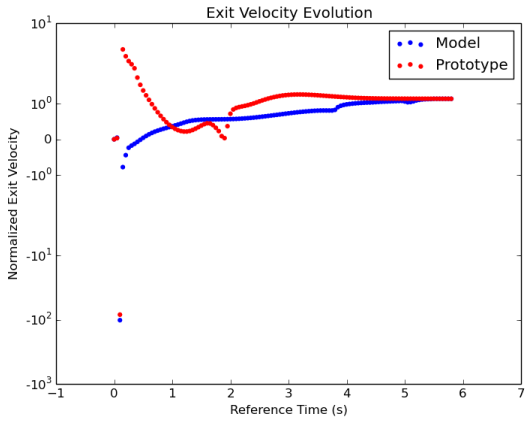


Figure 30 Exit velocity evolution of derived ideal case ($\omega$-strain scaling).

Overall, the draining tank $\omega$-strain scaling detected anomalies in the ideal case and found better agreement in model cases with prototypic tank heights. Possible pressure effects due to different tank heights may be adding error to gravity driven assumptions. Also, the issue concerning the pressure differential discontinuity remains a problem in the $\omega$-strain scaling, and may be resolved by applying different initial hydrostatic pressures at every tank height (since it is modeled using the pipe component, this is possible by creating multiple partitions and setting different conditions).

Table 7. $\omega$-Strain water level and exit velocity standard errors for each sampled case.

| Samples | Tank Height (m) | Water Level Standard Error | Exit Velocity Standard Error |
|---|---|---|---|
| 0 | 22.461 | 2.611e-1 | 21.693 |
| 1 | 19.980 | 2.307e-1 | 25.032 |
| 2 | 31.317 | 5.892e-1 | 20.871 |
| 3 | 22.698 | 2.644e-1 | 20.350 |
| 4 | 14.915 | 9.478e-2 | 21.239 |
| 5 | 1.036 | 5.490 | 3.348 |
| 6 | 26.305 | 5.947e-1 | 19.636 |
| 7 | 24.591 | 5.878e-1 | 20.987 |
| 8 | 15.290 | 4.155e-2 | 21.193 |
| 9 | 25.014 | 5.885e-1 | 21.013 |
| Ideal | 7.000 | 1.897e-1 | 9.126 |

## 6. Conclusion and Future Work

The DSS has been successfully implemented and verified in the RAVEN code framework. The purpose of the verification study was to test the capabilities of DSS RAVEN code with a simple external code and engage meaningful conclusions that may improve simulation model selections and geometric dimensions. The DSS code written for RAVEN is a compilation of DSS derived postprocessing algorithms with modifications implemented to prevent data processing errors. The code receives time-dependent data for multiple parameters per user request and will notify the user when insufficient inputs are provided. For the case of this gravity-driven draining tank problem, two parameters were chosen to postprocess: water level and exit velocity. Equations were derived and non-dimesionlized in the form accepted by the DSS theory, and two separate time scaling methods were chosen to demonstrate the types of postprocessing response: identity and $\omega$-strain. After calculating relevant values to enable the RELAP5-3D input deck to run with a range of initial and boundary conditions, the RAVEN input file was written with the workflow illustrated in Figure 5. Both identity and $\omega$-strain.input files ran successfully, providing 10 samples each for the model and prototype to send to the DSS code. DSS postprocessed data revealed that the input deck written for RELAP5-3D showed strong dependencies in the water tank height and outputting maximum exit velocities around the size of the derived reference value. Although RELAP5-3D managed to rectify the issue, by water level and exit velocity investigation, discontinuous differential pressure was found in the first few hundred milliseconds and affected velocity calculations enough to yield unrealistic values. It is suggested to modify the input deck to account for hydrostatic pressure as an initial condition to avoid further discontinuities in data not triggered by breaks or trips. In addition to initial findings, the DSS code was capable of dealing with NaN and infinite values (products of dividing by 0) and correctly alleviated the issue by nullifying local separation values at reference times known to have the problem values. The DSS code implementation into RAVEN was a success for the given example simulations and functioned as anticipated.

Due to the delay of the TEDS facility data generation and complexity to obtain a nonproprietary RELAP5-3D PWR input deck to sample, the application of DSS RAVEN code to existing facilities is planned for as soon as TEDS data becomes available. For the next fiscal year, the facility application is planned, and possible facility or test design optimizations will be attempted. For data extrapolation, a new DSS postprocessor will be written within RAVEN.

# References

[1] Stoots, C., D.M. Duenas, P. Sabharwall, J. O'Brien, J. Soo Yoo, and S. Bragg-Sitton. 2018. "Thermal Energy Delivery System Design Basis Report." INL/EXT-18-51351-Rev000, Idaho National Laboratory. https://doi.org/10.2172/1756571.

[2] Reyes, J. Jr. 2015. "The Dynamical System Scaling Methodology." In The 16th International Topical Meeting on Nuclear Thermal Hydraulics (NURETH-16), August 30–September 4, Chicago, IL, 177–191. http://glc.ans.org/nureth-16/data/index.htm.

[3] Martin, R.P., and C. Frepoli, eds. 2019. *Design-Basis Accident Analysis Methods for Light-Water Nuclear Power Plants*. World Scientific. https://doi.org/10.1142/11139.

[4] Yoshiura, R.K. 2021. "Dynamic System Scaling Application to Accelerated Nuclear Fuel Testing," Ph.D. diss., Oregon State University. https://ir.library.oregonstate.edu/concern/parent/br86bb53b/file_sets/9g54xr31j.

[5] Idaho National Laboratory. N.d. "Risk Analysis Virtual Environment – RAVEN." https://github.com/idaholab/raven/wiki/docs/Pop-up-Backdrop-RiskAnalysisVirtualENviroment-flyer.pdf

[6] Li, X., N. Li, Q. Wu, H. Zhang, A. Samad Muhammad, and D. Lu. 2019. "Application of dynamical system scaling method on simple gravity-driven draining process." Journal of Nuclear Science and Technology 55(1): 11–18. https://doi.org/10.1080/00223131.2017.1372231.

[7] Sabharwall, P., J. E. O'Brien, M. G. McKellar, G. K. Housley, S. M. Bragg-Sitton, and R. D. Boardman. *Scaling Analysis Techniques to Establish Experimental Infrastructure for Component, Subsystem, and Integrated System Testing*, INL/EXT-15-34456, Idaho National Laboratory, Idaho, March 2015.

[8] A. Epiney, C. Rabiti, C. Davis, "A Systematic Approach to Inform Experiment Design Through Modern Modelling and Simulation Methods", Proceedings NURETH-18 conference, Portland, OR, August 18-22, 2019.

[9] Hany S. Abdel-Khalik, Ayman I. Hawari, and Congjian Wang, "Physics-guided Coverage Mapping (PCM): A New Methodology to Avoid Model Calibration," 7th Intl. Conf. on Modelling and Simulation in Nuclear Science and Engineering, Ottawa, October, 2015; and Intl. Conf. on Mathematics and Computation, Nashville, TN, April, 2015.